

Angle-resolved photoemission study of the surface and bulk electronic structure of Mg(0001) and Mg(11 $\bar{2}$ 0)

R. A. Bartynski

Department of Physics and the Laboratory for Research on the Structure of Matter, University of Pennsylvania, Philadelphia, Pennsylvania 19104

R. H. Gaylord

Department of Material Science and Engineering and The Laboratory for Research on the Structure of Matter, University of Pennsylvania, Philadelphia, Pennsylvania 19104

T. Gustafsson and E. W. Plummer

Department of Physics and The Laboratory for Research on the Structure of Matter, University of Pennsylvania, Philadelphia, Pennsylvania 19104

(Received 3 September 1985)

Angle-resolved ultraviolet photoemission spectroscopy measurements have been made from the (0001) and (11 $\bar{2}$ 0) surfaces of magnesium in the photon energy range of 15 to 115 eV. Both bulk and surface features are identified. The occupied bands along the [0001] direction are characterized by the measured energy eigenvalues at the Γ point: $\Gamma_1^+ = 6.15 \pm 0.1$ eV, $\Gamma_3^+ = 1.7 \pm 0.1$ eV, and $\Gamma_4^- = 0.9 \pm 0.1$ eV. The bandwidth, as measured for both the (0001) and the (11 $\bar{2}$ 0) surfaces, is 10% smaller than that predicted by band-structure calculations, while the $\Gamma_3^+ - \Gamma_4^-$ band gap is twice as big as calculated. The narrower experimental bandwidth is related to the fact that the excitation spectrum of the system is measured, while the origin of the wider experimental gap is not as clear. The final states higher than 28 eV above E_F are well described by a free-electron band of effective mass $m^*/m = 1.04$, originating 6.15 eV below the Fermi level, while the low-energy final states deviate greatly from free-electron-like behavior. The peak widths of the bulk features in both the [0001] and the [11 $\bar{2}$ 0] direction are significantly larger than predicted by interacting electron-gas theory. The peak widths along [0001] increase near the middle of the band, due to final-state effects. The binding energy of the $\bar{\Gamma}$ surface state on the (0001) surface has been redetermined to be 1.6 ± 0.1 eV. A surface state at \bar{M} has a binding energy of 1.1 ± 0.1 eV. The $\bar{\Gamma}$ surface state shows a sharp intensity resonance near $\hbar\omega = 44$ eV giving the location of a state of Γ_4^- symmetry in the final state. The \bar{M} surface state shows a similar resonance near $\hbar\omega = 26$ eV. The surface-state dispersions have been measured in the $\bar{\Gamma} - \bar{M}$ direction.

INTRODUCTION

Angle-resolved ultraviolet photoelectron spectroscopy data from single crystals are often interpreted in terms of the bulk electronic band structure.¹ Such an interpretation is based on several assumptions. Firstly, photoemission is a process which probes excitations while band-structure calculations describe ground-state properties. Secondly, band-structure calculations are inherently one-electron descriptions of the electronic structure; any electron-electron interactions in the ground state, beyond mean-field effects, are ignored. Finally, the eigenvalues of a band-structure calculation have no formal interpretation in terms of electron energies and are only meaningful in the context of total energies. Experimentally, the vast majority of photoemission studies of single-crystal metals have been performed on the transition and noble metals.¹ There has usually been quite good qualitative agreement between theory and experiment. The origin of the quantitative discrepancies that do exist is often obscured by the complexities involved in theoretically describing the d electrons. These problems have motivated us to use pho-

toelectron spectroscopy to investigate the electronic structure of simple metals. These materials have no occupied d states and will allow the validity of the aforementioned assumptions to be explored in a more direct way.

Reports from this laboratory of angle-resolved photoemission measurements of the surface and bulk electronic structure of Al and Be have appeared earlier.^{2,3} In the present paper we extend this work to Mg. We present extensive data from the (0001) face which show both bulk and surface features. Since the surface-state signal dominates interesting bulk transitions for certain photon energies, we have also studied emission from the (11 $\bar{2}$ 0) face. No band gaps exist in this direction and consequently no surface-state emission. We will compare our results to those from Al and Be where appropriate,^{2,3} and point out certain trends which occur in these systems.

In general, peak positions in the normal emission spectra from both Mg(0001) and Mg(11 $\bar{2}$ 0) are qualitatively well described by direct transitions between one-electron band states. However, on a quantitative level, we find that there are significant numerical differences in the occupied band structure between state of the art calcula-

tions⁴ and experiment, both for the bandwidth and the band gaps. The occupied bandwidth, predicted by self-consistent pseudopotential calculations⁴ to be 6.8 eV, is measured to be 6.15 ± 0.1 eV, some 10% smaller than calculated. Two states at Γ with Γ_3^+ and Γ_4^- symmetry span a band gap along Δ . We have measured their binding energies to be 1.7 ± 0.1 eV and 0.9 ± 0.1 eV, respectively. Consequently, the $\Gamma_3^+ - \Gamma_4^-$ gap is 0.8 eV wide, while most theoretical estimates are around 0.4 eV.⁴⁻¹²

For final-state energies less than 25 eV above the Fermi energy (E_F) the bulk bands are described poorly by a free-electron parabola. This is an energy region where the $2p$ core level photoabsorption spectrum¹³ shows evidence for d -derived states. At higher energies, free-electron-like final states with an effective mass of $m^*/m = 1.04$ describe the data quite well. Even better agreement is achieved when the data are compared to (rigidly shifted) self-consistent calculations.⁴

We also report new data on the position and dispersion of a surface state in the $\Gamma_3^+ - \Gamma_4^-$ gap on the hexagonal (0001) face, the existence of which was first reported by Karlsson *et al.*¹⁴ This state has a binding energy of 1.6 eV at $\bar{\Gamma}$, which places it 0.1 eV into the gap. The state disperses so that it tracks the lower band edge. It shows a sharp intensity resonance near $\hbar\omega = 44$ eV, associated with transitions to a Γ_4^- state in the final bands, placing this energy level 42 eV above E_F .

The bulk peak widths observed for both Mg(0001) and Mg(11 $\bar{2}$ 0) are much greater than those predicted by interacting electron-gas calculations,¹⁵ though they do follow the expected trend in that they decrease as the Fermi level is approached. For Mg(0001), deviations from a monotonic behavior are seen for transitions to a flat final band near a band gap. This indicates that band structure effects might be important in understanding photoemission peak widths. This anomalous behavior is not observed in normal emission from Mg(11 $\bar{2}$ 0) where the final bands are free-electron-like.

EXPERIMENTAL

All experimental data were obtained at the Synchrotron Radiation Center of the University of Wisconsin—Madison, in Stoughton, Wisconsin on the Tantalus II storage ring. The incident radiation in the energy range $15 \text{ eV} < \hbar\omega < 120 \text{ eV}$ was dispersed with a toroidal grating monochromator¹⁶ with a plane of dispersion chosen to enhance the polarization of the synchrotron light. The monochromator was coupled to a μ -metal shielded ultrahigh-vacuum (UHV) sample chamber. The photon flux incident on the sample was monitored with a highly transparent tungsten mesh mounted between the last optical element of the monochromator and the sample. The photoemitted electrons were collected by a 180° hemispherical electrostatic analyzer with an acceptance angle of $\pm 2.5^\circ$.¹⁷ The analyzer is mounted on a two-axis goniometer, allowing independent variation of the polar and azimuthal angles of electron collection. The total energy resolution, due both to the spread in photon and in electron energies, varied from 0.1 to 1.0 eV throughout this photon energy range, but was typically 0.3 eV in or-

der to maintain reasonable count rates.

The UHV chamber also contained a low-energy electron diffraction (LEED) system for sample orientation and characterization. A commercial double-pass cylindrical mirror analyzer was used for Auger electron spectroscopy (AES) to monitor surface cleanliness.

The Mg(0001) and Mg(11 $\bar{2}$ 0) samples were cut from a single boule of 99.98%-pure single-crystal Mg. The boule was oriented to within 3° by Laue diffraction and then spark cut. The resulting slice was then reoriented and polished to within 1° using a South Bay Technology crystal facer. Mechanical polishing to 0.05- μm grit was followed by electropolishing with a 30 vol% solution of phosphoric acid in ethanol.

Once inserted in the vacuum chamber, the samples were cleaned with several 1-h cycles of sputtering (1 keV Ne, 10 $\mu\text{A}/\text{cm}^2$) followed by annealing at 200°C for 10 min. This procedure produced good quality LEED patterns at room temperature. At liquid-nitrogen temperature the LEED pattern became quite sharp and the background was reduced. Care was taken to keep the sample temperature below 250°C at all times to avoid evaporation. After preparation as described above, the photoemission spectra showed a large oxygen signal even though AES indicated a clean surface. This oxide layer was removed by a single sputtering cycle at $\approx 150^\circ\text{C}$ followed by a 5-min anneal at 200°C. With this additional step in the cleaning procedure, the photoelectron spectra showed no trace of oxygen for several hours at our operating pressure of 2×10^{-10} torr. The crystal surface, which was mirrorlike after electropolishing, was macroscopically hazy after sputtering. In spite of this fact, a good LEED pattern with no indication of faceting could be obtained, and photoemission from the Mg(0001) surface state showed the correct two-dimensional periodicity.

The crystal structure of Mg is hexagonally close packed (hcp) with (conventional) real- and reciprocal-space unit cells as shown in Fig. 1. The notation of Herring¹⁸ is used. For reference, a qualitative plot of the band structure of Mg along several high-symmetry directions of the Brillouin zone is also presented.¹² The unit cell contains two atoms, which implies that there is no first-order splitting of the energy bands along the hexagonal $A-H-L$ plane of the Brillouin zone (BZ). The (0001) surface corresponds to the hexagonal basal plane. Normal emission from the (0001) surface explores the states along the Δ ($\Gamma-A$) direction of the Brillouin zone. Only initial states of Δ_1 or Δ_2 symmetry can couple to final states detectable in this geometry. Furthermore, only $\Delta_1 \rightarrow \Delta_1$ and $\Delta_2 \rightarrow \Delta_2$ transitions are allowed by symmetry. This allows us to unfold the bands about the A point and plot the bands as a function of \mathbf{k} along $\Gamma-A-\Gamma$ (see Fig. 7).

The (11 $\bar{2}$ 0) surface has a rectangular unit mesh. In real space this surface corresponds to zig-zagging rows of close-packed atoms. It is a rather open structure with low symmetry. There is only one mirror plane that contains the surface normal. This is the plane formed by the surface normal and the $\bar{\Gamma}-\bar{M}$ direction. Normal emission from this surface investigates the bands along the T ($\Gamma-K$) direction. In the extended BZ this line continues with T' ($K-M$). This means that, in normal emission

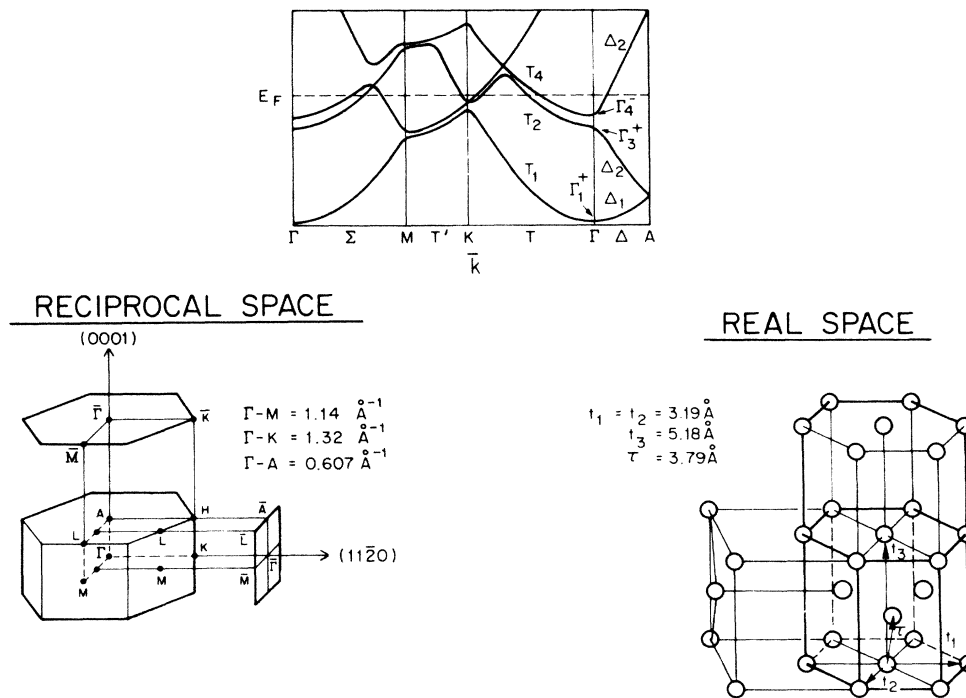


FIG. 1. The real- and reciprocal-space lattice of hcp Mg. The projections for both the (0001) and the (11 $\bar{2}$ 0) surfaces are shown. The top half of the figure shows a plot of the band structure after Ref. 12.

from this surface, one probes states along $\Gamma\text{-K-M}$. States of T_1 symmetry are the only initial states seen in normal emission from this surface. The band structure in Fig. 1 shows that the lowest band is free-electron-like, originating at Γ_1^+ . One can consequently measure the bandwidth from this surface also. The bands in Fig. 1 show that a small gap opens up at K , but since both the upper and lower bands disperse downwards from K to M , there is on this surface no projected gap in normal emission.

All binding energies and kinetic energies reported in this paper are referenced to $E_F=0$ eV. All peak widths reported are full width at half maximum (FWHM).

RESULTS

Normal emission spectra obtained from Mg(0001) at various photon energies are shown in Fig. 2. The dominant feature in the $\hbar\omega=23$ eV spectrum seen at approximately 4-eV binding energy is emission from a Mg $2p$ core level excited by third-order radiation from the monochromator. By $\hbar\omega=26$ eV this peak is seen above E_F and no longer interferes with the first-order valence-band spectrum. Another intense peak enters the spectrum near $\hbar\omega=40$ eV and moves rapidly towards the Fermi level as the photon energy is increased. This is emission from the same $2p$ core level excited by second-order radiation. The relative intensities of the higher-order core levels and the first-order valence band is indicative of the low valence-band cross section.

A prominent feature in the primary spectrum for most normal emission spectra occurs at 1.6-eV binding energy.

The spectra in Fig. 2 show that the binding energy of this peak does not change with photon energy over the range investigated. In addition it shows sensitivity to surface contamination. Karlsson *et al.*¹⁴ have previously observed this feature and attributed it to emission from a surface state in the $\Gamma_3^+-\Gamma_4^-$ bulk band gap. Our observations confirm this assignment. As discussed below, our measurements from bulk emission gives $\Gamma_3^+=1.7$ eV placing the surface state 0.1 eV into the gap.

It is evident from Fig. 2 that the surface-state intensity is a strong function of $\hbar\omega$. This observation is quantified in Fig. 3 where the surface-state intensity is plotted as a function of photon energy. The intensity profile has two main features: a small resonance near $\hbar\omega=23$ eV and a much stronger one near $\hbar\omega=43$ eV. These enhancements are related to strong coupling to the final states at these photon energies.

As the electron analyzer is moved away from the surface normal, states with nonzero momentum parallel to the surface ($k_{||}$) are investigated. The quantity $k_{||}$ is conserved in the photoemission process and may be related to the photoelectron emission angle by the equation

$$k_{||} = \sqrt{2mE_k/\hbar^2} \sin\theta_E, \quad (1)$$

where $E_k = \hbar\omega - E_B - \phi$ is the kinetic energy of the emitted electron, ϕ the work function, and θ_E is the angle at which the electron is emitted. Spectra taken at $\hbar\omega=26$ eV for increasing polar angle along the $\bar{\Gamma}\text{-}\bar{M}$ azimuth of the Mg(0001) surface are shown in Fig. 4. The features which occur below 2-eV binding energy are attributed to

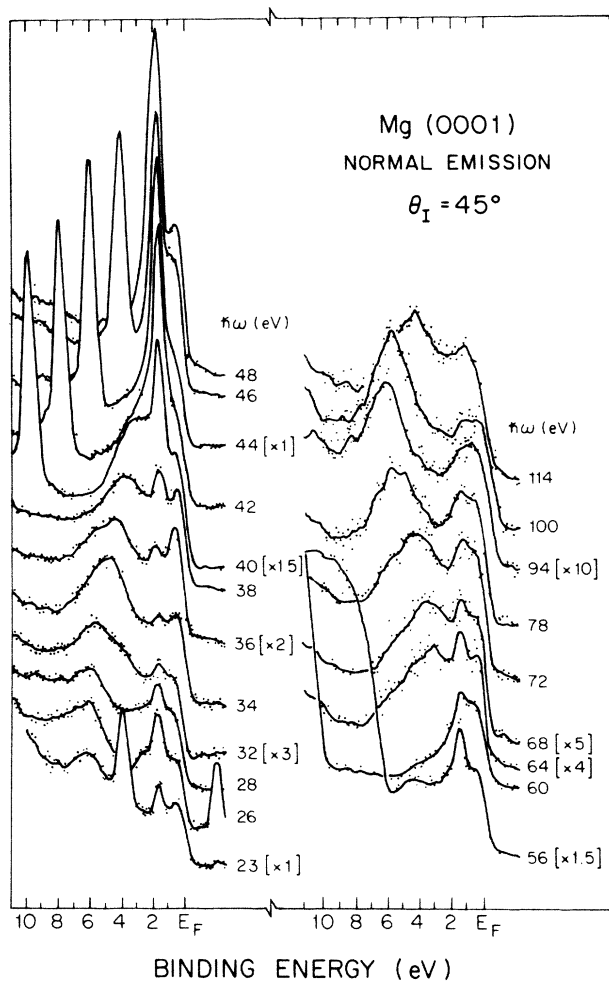


FIG. 2. Normal emission photoelectron spectra from the Mg(0001) surface taken at various photon energies. The angle of the incident light was 45° from the sample normal. In this and other figures containing spectra, the raw data (dots) have been digitally smoothed to generate the solid curves.

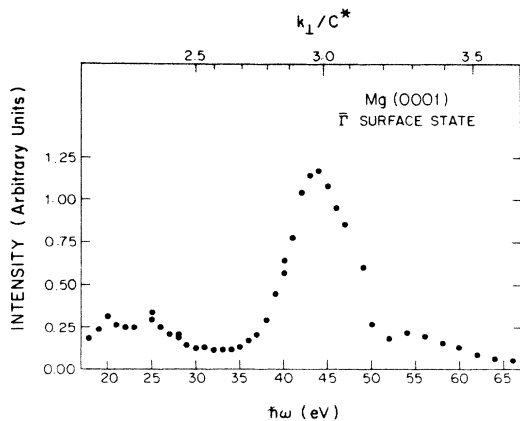


FIG. 3. The normalized intensity of the Mg(0001) surface state. The lower horizontal scale gives the photon energy while the upper horizontal scale gives the parallel momentum assuming free-electron-like final states with an effective mass of $m^*/m = 1.04$ originating 6.15 eV below E_F .

bulk emission and will not be discussed here. The surface state at $\bar{\Gamma}$ has a binding energy of 1.6 eV and disperses towards E_F as the emission angle moves away from normal. The state crosses the Fermi level near $\theta = 18^\circ$. As the angle is increased further, another large peak is seen crossing E_F and then dispersing downward, reaching a maximum binding energy of 1.1 eV near $\theta = 30^\circ$. This feature then disperses upward again reaching the Fermi level near $\theta = 49^\circ$. For larger angles, the surface states seen near normal emission returns below E_F and disperses down-

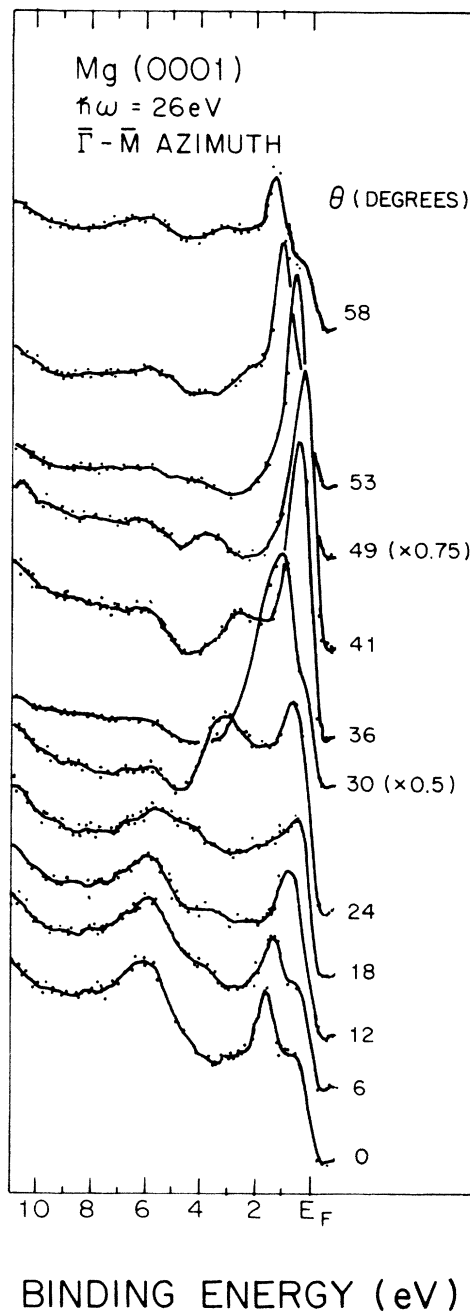


FIG. 4. Photoelectron spectra from Mg(0001) taken at various angles along the $\bar{\Gamma}-\bar{M}$ azimuth at a photon energy of 26 eV. The angle of incidence was 45°. Note that the 30° and 49° spectra are reduced to fit on the figure.

ward as $\bar{\Gamma}$ in the second surface Brillouin zone (SBZ) is reached.

The dispersion of these features may be more clearly discussed when the binding energy is plotted versus k_{\parallel} as is presented in Fig. 5. The data in this figure include results obtained at $\hbar\omega=40$ and 43 eV as well as those shown in Fig. 4. Also plotted in this figure are the projected bulk bands for the Mg(0001) surface as determined from a calculation by Chou and Cohen.⁴ The dispersion of the surface state clearly follows that of the projected band edge, and both are fitted by a free-electron-like parabola with an effective mass of $m^*/m=1.31$. The feature which has a maximum binding energy of 1.1 eV shows a symmetric dispersion about the \bar{M} point of the SBZ and exists in a bulk band gap. This is the \bar{M} surface state seen by Karlsson *et al.*¹⁴ The symmetric dispersion and the maximum binding energy are reported here for the first time. When the surface state from normal emission reappears below E_F at $k_{\parallel}=1.6 \text{ \AA}^{-1}$, its dispersion about $\bar{\Gamma}$ in the second SBZ, including the effective mass and binding energy, is the same as in the first SBZ.

Returning to Fig. 2, a rather broad but distinct peak occurs at a binding energy of 6.15 eV at $\hbar\omega=23$ eV and then disperses toward E_F as the photon energy increases. By $\hbar\omega=44$ eV the deeper peak is no longer separable from the strong emission from the surface state. Near $\hbar\omega=38$ eV, a second peak appears at the Fermi level and disperses downward toward the surface state. This peak reaches its maximum binding energy near $\hbar\omega \approx 43$ eV and then disperses back towards the Fermi level, crossing it again near $\hbar\omega=47$ eV. Near $\hbar\omega=43$ eV, the dispersing peak is difficult to resolve from the surface state. When the line shape at $\hbar\omega=43$ eV is fitted with two Gaussians, a binding energy of 0.9 ± 0.1 eV is obtained for the dispersing feature. This is the deepest binding energy measured. The same value is obtained by extrapolating the dispersion of this feature from the $\hbar\omega=38\text{--}42$ eV range to the $\hbar\omega=45\text{--}47$ eV range. We therefore feel quite confident that the peak reaches a maximum binding energy of 0.9 ± 0.1 eV at $\hbar\omega \approx 43$ eV.

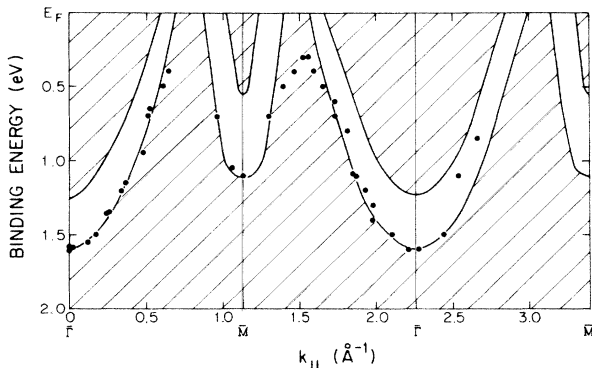


FIG. 5. The binding energy of the Mg(0001) surface state as a function of parallel momentum. The dots represent data taken from spectra obtained at $\hbar\omega=26$, 40, and 43 eV. The shaded region depicts the projected bulk bands as determined from Ref. 4.

In the photon energy range of $50 \text{ eV} < \hbar\omega < 58 \text{ eV}$ the valence spectrum is dominated by Auger electrons generated by $2p$ core excitation. This emission is seen as the large intensity at high binding energy in the 56 and 60 eV spectra. A small peak is visible at 4 eV in the $\hbar\omega=56$ eV spectrum and near the Fermi level in the $\hbar\omega=60$ eV spectrum. The change in kinetic energy of this feature with $\hbar\omega$ indicates that it is excited by second-order radiation. Its kinetic energy is consistent with it being a plasmon loss off the second-order $2p$ core level. The only discernible true valence-band features in this energy range are the Fermi level and the surface state. This remains true for the next 10 eV of photon energy although the Auger electrons have moved well out of the spectrum and no longer interfere. Near 65 eV emission from the bulk feature below the surface state becomes evident again and the peak disperses downward with photon energy. It reaches a maximum binding energy of 6.15 eV near $\hbar\omega=95$ eV, then turns around and starts dispersing toward E_F at higher photon energies.

The dispersion of these peaks with photon energy is more clearly seen when their binding energy is plotted versus $\hbar\omega$ as in Fig. 6. The high binding-energy peak remains essentially dispersionless for approximately 10 eV before it starts moving toward the Fermi level. There is a clear region in binding energy where no dispersing peaks exist and only the surface state is present. For a small range of photon energies between 39 and 48 eV, the low binding-energy peak makes a brief excursion below E_F and then does not appear again. At high $\hbar\omega$ the high binding-energy peak reaches the same maximum binding energy of 6.15 eV. Also shown in Fig. 6 are the peak positions from the Mg(11 $\bar{2}$ 0) normal emission spectra. The spectra from which these points are obtained are very similar to those of Fig. 2 (but without the surface state) and, therefore, are not shown. As mentioned above, only one band is explored in normal emission from this surface. The peak corresponding to transitions from this band reaches a maximum binding energy of 6.15 ± 0.1 eV.

Within the framework of a direct transition model, extrema in a plot of binding energy versus photon energy correspond to symmetry points in the band structure. The band bottom, given by Γ_1^+ , is measured from the (0001) data below $\hbar\omega=30$ eV and near $\hbar\omega=90$ eV as 6.15 ± 0.1 eV. The data from the (11 $\bar{2}$ 0) surface near $\hbar\omega=60$ eV confirm this result. To our knowledge, this is the first time a bandwidth has been measured with photoemission from two different surfaces of the same material. This shows that the positions of bulk valence-band features in photoemission are independent of the surface from which they are measured.

From the maximum binding energy near $\hbar\omega=43$ eV of the low binding-energy state we find $\Gamma_4^- = 0.9 \pm 0.1$ eV. It is hard to establish the minimum binding energy of the deeper peak from the (0001) data. The reason for this is evident from Fig. 2. Near $\hbar\omega=40$ eV, as the bulk peak approaches its minimum binding energy, the surface-state intensity is very large making the bulk peak indistinguishable from the surface-state emission. Consequently, we refrain from quoting an energy for the Γ_3^+ state from the (0001) data alone.

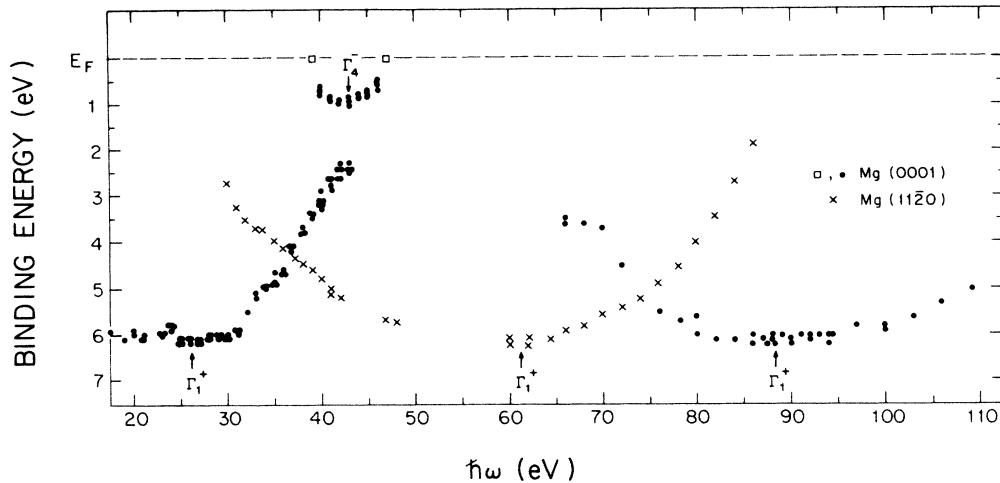


FIG. 6. Binding energy versus photon energy of the dispersing peaks observed in normal emission spectra from the Mg(0001) (represented by ● and □) and the Mg(11 $\bar{2}$ 0) (represented by ×) surfaces. The energies of levels of high symmetry in the bulk band structure are identified as extrema in this dispersion.

The (11 $\bar{2}$ 0) surface has no band gaps in normal emission. This allows one to study the initial-state band without interference from surface-state emission. Figure 1 shows that the Γ_3^+ state lies on a band of T_2 symmetry. As only bands of T_1 symmetry are seen in normal emission, it is necessary to go to $\bar{\Gamma}$ in the second surface Brillouin zone [$\bar{\Gamma}(2)$]. The low symmetry of this surface prevents the identification of states via selection rules. Instead, we employ the same technique as was used to locate symmetry points at normal emission: The photon energy is varied as $k_{||}$ is held fixed and extrema in the peak dispersion are sought. When $\theta_E \neq 0^\circ$, $k_{||}$ changes as the photon energy is varied; thus, the collection angle of the detector has to change with photon energy to remain at the $\bar{\Gamma}(2)$ point. The spectra in this region of k space contain one peak which remains close to the Fermi level. The maximum binding energy (1.7 eV) is reached at $\hbar\omega = 55$ eV.

To ensure that this is the Γ_3^+ energy level, the behavior of the peak was examined in the region of k space near the $\bar{\Gamma}(2)$ point. The top half of Fig. 7 shows the topology of the bands near the $\bar{\Gamma}$ point. The figure illustrates how the bands disperse toward the Fermi level when one moves in any direction away from Γ_4^- . From Γ_3^+ , however, the bands disperse downward along $\Gamma \rightarrow A$. The spectra plotted in the lower half of Fig. 7 show the motion of the peak as $k_{||}$ is varied along $\Gamma \rightarrow A$ at fixed photon energy. The peak is clearly dispersing downward as k moves away from $\bar{\Gamma}$. When $k_{||}$ is varied along $\Gamma \rightarrow M$, the peak seen in Fig. 7 disperses toward E_F . The binding energy of the saddle point is measured as 1.7 ± 0.1 eV, giving this value for Γ_3^+ .

Since the photoemission process does not conserve momentum perpendicular to the surface, a value of k_{\perp} cannot usually be assigned unambiguously to an observed peak. However, data from other techniques may be used in conjunction with photoemission results to arrive at

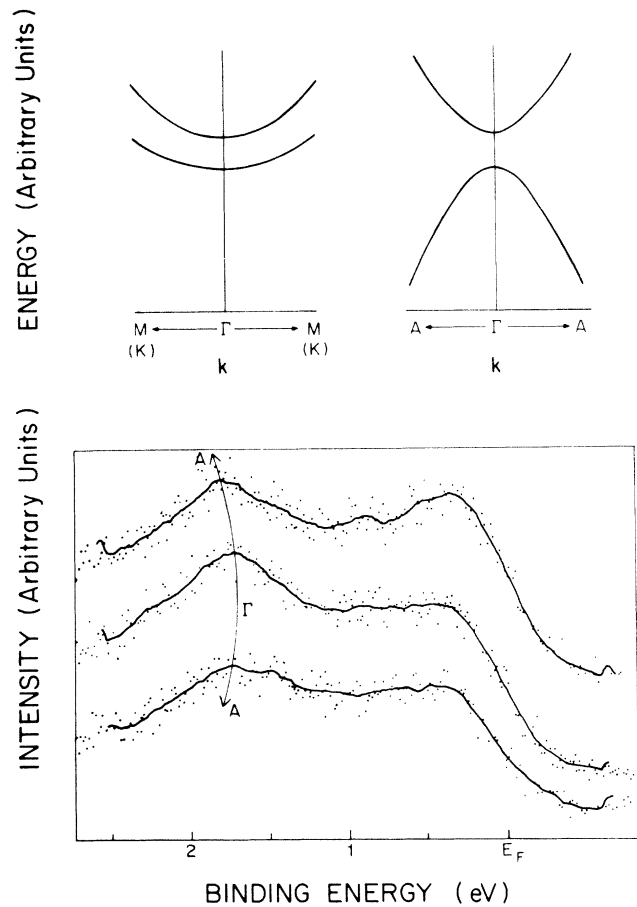


FIG. 7. Schematic plot of the Mg band structure near the Γ_3^+ and Γ_4^- energy levels (upper panel). Energy distribution curves taken near Γ_3^+ in the second SBZ along $\Gamma-A$ with p -polarized light are shown in the lower panel.

unique values of k_{\perp} for certain peaks. For example, the Fermi-surface topology of Mg has been very accurately measured from de Haas—van Alphen¹⁹ and magnetoacoustic attenuation data.²⁰ Consequently, if a transition occurs from the Fermi level, one can obtain the correct k_{\perp} from these data and then assign E and k_{\perp} for the photoemission data directly. From Figs. 2 and 6 we observe that the low binding-energy peak crosses the Fermi level at two photon energies. In Fig. 8 we plot the intensity at the Fermi level as a function of photon energy. This plot shows an absolute maximum at $\hbar\omega = 47$ eV and a subsidiary maximum at $\hbar\omega = 39$ eV. These points correspond to the Fermi-level crossings of the upper partially occupied band. From the Fermi-surface parameters determined from de Haas—van Alphen data,²⁰ we find that the wave vector of this transition is 0.152 \AA^{-1} . This establishes the k_{\perp} for the final states reached in these transitions. We have therefore located two points in the final-state band structure at $k_{\perp} = 0.152 \text{ \AA}^{-1}$ with energies of 39 and 47 eV above E_F .

The line shapes and peak widths in photoemission are important in understanding the lifetimes of the states involved.²¹ In Fig. 9 we show the FWHM for peaks associated with the deeper bulk peak for transitions from the (0001) and the (11 $\bar{2}$ 0) surfaces. The data are plotted as a function of the reduced wave vector k/k_F as this facilitates a comparison with theory. The data have not been corrected for the contribution of the finite experimental resolution to the peak widths, but since the observed widths are much greater than the instrumental resolution, this will have no effect on the points discussed below. There is a fair amount of scatter in the (0001) data near the band bottom. This is due to final-state contributions to the peak width which occur between $\hbar\omega = 18$ and 28 eV when the peak is not yet dispersing. Just prior to dispersing, the peak width at the band bottom is approximately 2.2 eV on both surfaces. As $k/k_F \rightarrow 1$, the peak widths along the [11 $\bar{2}$ 0] direction remain essentially constant un-

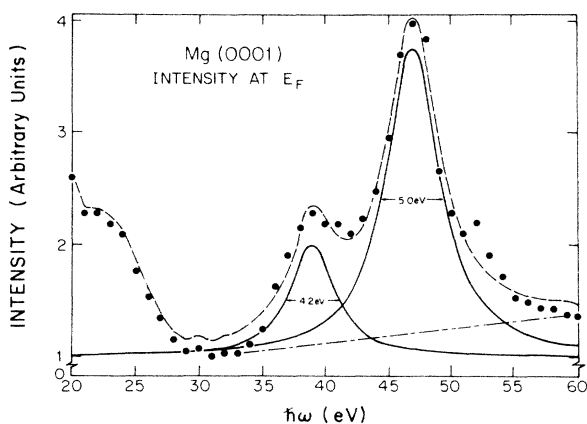


FIG. 8. Intensity at the Fermi level as a function of photon energy for the normal emission spectra from the Mg(0001) surface. The two Lorentzians (solid curves) added to a linear background (dot-dash line) result in a best fit to the data (dashed curve).

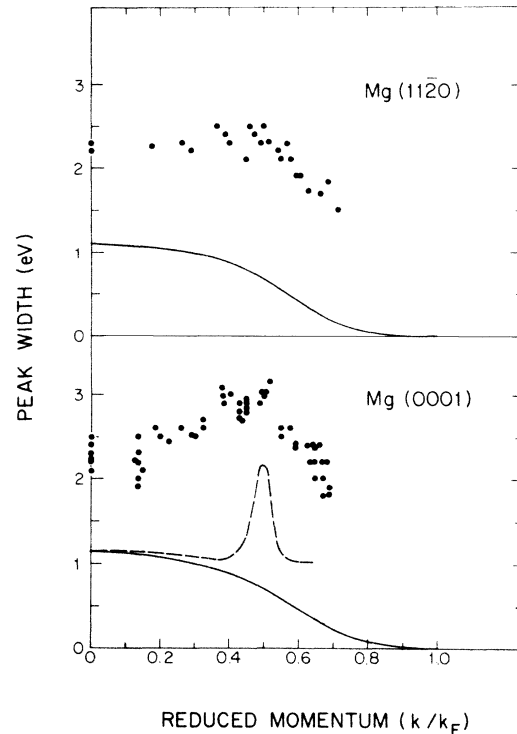


FIG. 9. Bulk peak width as a function of reduced momentum (k/k_F) ($k_F = 3.18 \text{ \AA}^{-1}$) for normal emission for the Mg(0001) and Mg(11 $\bar{2}$ 0) surfaces. The solid line represents the prediction for an interacting electron gas of the same density as Mg ($r_s = 2.66$). The dashed curve shows the calculated influence of the final states along the [0001] direction.

til $k/k_F \approx 0.5$ and then decrease smoothly. In the [0001] direction, however, the widths show a distinct increase, reaching a maximum of about 3.2 eV in the range $0.4 < k/k_F < 0.5$, and then dropping off again as k/k_F approaches unity. The direct transition close to the Fermi level has too little intensity and resides on too large a background to give meaningful results.

DISCUSSION

The occupied bandwidth and the band gaps

The photoemission process does not conserve perpendicular momentum k_{\perp} , so some assumptions must usually be made in order to arrive at a band structure. The occupied bands of Mg along $\Gamma \rightarrow A$, however, are quite simple and are essentially characterized by the measurement of the energy levels at Γ . The results of the previous section showed that $\Gamma_1^+ = 6.15$ eV, as given by the bandwidth. A free-electron calculation for the density of Mg ($r_s = 2.66$) gives a bandwidth of 7.1 eV. Early band-structure calculations showed little change, yielding a bandwidth of 7.0 eV.⁵⁻⁷ Later first-principles calculations concentrated on improving the agreement with Fermi-surface data and resulted in almost no change in the bandwidth.⁸⁻¹⁰ Modern, self-consistent calculations place Γ_1^+ at 6.9 eV,^{11,12} while a recent self-consistent pseudopotential cal-

ulation employing the local-density approximation⁴ (LDA) places Γ_1^+ at 6.8 eV. The general agreement among these calculations seems to indicate that, within the LDA, factors such as self-consistency, a sophisticated treatment of exchange and correlation or improvement in the numerical accuracy of the calculation have little influence on the calculated bandwidth.

The experimentally measured bandwidth for aluminum² and sodium²² is also narrower than theoretically calculated, while the agreement for beryllium³ is quite good. Copper has a measured bandwidth of 8.6 eV,²³ 14% smaller than the 10 eV bandwidth predicted by local-density calculations.²⁴

Assuming the validity of the band picture, there may be two causes for this disagreement: deficiencies in the local-density approximation or inaccuracies inherent in comparing an excitation spectrum with a ground-state calculation. The local-density functional is an approximation to the true many-particle potential for the ground state. In the local-density approximation for exchange and correlation there is not complete cancellation of the Coulombic self-interaction.²⁵ This double counting of energies shifts the calculated bands from those based on the exact density functional ground state. One may include self-interaction corrections (SIC) in the potential, yielding eigenvalues which closely correspond to relaxed removal energies. The improved agreement with experiment is the result of nearly complete cancellation of the "non-Koopmans" corrections by the relaxation energy.²⁵ The resulting eigenvalues resemble those of the original local-density approximation calculation with slightly shifted energies. Self-interaction corrections have been applied to Cu (Ref. 26) band-structure calculations resulting in improved agreement with the bandwidth obtained from photoemission data, but poorer predictions for the *d* bands. A screened self-interaction correction improves the calculated *d* bands but gives poor results for the bandwidth.²⁶ No predictions have been made for the simple metals. Clearly, the self-interaction correction identifies shortcomings of the local-density approximation, but the actual implementation of the SIC is somewhat arbitrary at this stage, and the results are mixed.

One may address the differences between excitation spectra (which are measured by photoemission) and ground-state electron bands (calculated in a band-structure calculation) in terms of the self-energy for the interacting electron gas.¹⁵ Calculations of this property indicate it is momentum dependent and may be considered formally as a *k*-dependent term added to an exchange-correlation potential.¹⁵ The additional term results in only about a 5% contraction of the bandwidth for the electron density of Mg. Explicit inclusion of this term in a calculation of the spectral weight function for metallic Cu, taking into account the energy dependence of both the real and imaginary parts of the self-energy as given by the interacting electron gas, has resulted in a reduction of the bandwidth of a comparable magnitude.²⁷ In addition, similar discrepancies are observed for Na which has very delocalized electrons and a weak pseudopotential.²² The local-density approximation to the real density functional is therefore expected to get the ground-state bands quite

accurately for this material, yet experimentally a reduction of almost 20% is observed in the bandwidth.²² Again this reduction is considerably greater than predicted by electron-gas calculations.¹⁵ These results may indicate that the momentum-dependent self-energy is larger than expected from interacting electron-gas calculations, and may even be large enough to account for the bandwidth discrepancy we observe for Mg.

The remaining occupied states at Γ have measured binding energies of $\Gamma_3^+ = 1.7$ eV and $\Gamma_4^- = 0.9$ eV. The calculation of Chou and Cohen⁴ place these at 1.6 eV and 1.2 eV, respectively. There is some variation as to where the other calculations place these two band energies, but most yield a gap which is between 0.3 and 0.5 eV.⁴⁻¹² This means that the measured band gap is approximately twice as large as predicted by the calculation. The origin of this disagreement is not clear. Discrepancies of the same kind are observed in Al and Be (Refs. 2 and 3, respectively). Similarly, the measured fundamental band gaps in semiconductors are considerably different from the calculated ones.^{28,29} There are several different effects that can influence this. Self-energy terms for the electron gas give corrections to the band structure, the size of which increase monotonically with binding energy. The binding energy of the Γ_3^+ point would therefore be reduced more than that of the Γ_4^- point. This would, however, lead to an experimental band gap *smaller* than that calculated by local density theories, opposite to what is observed experimentally. The remaining explanation is the deficiencies in the *local* approximation itself. Attempts to improve agreement for the gap width of semiconductors by incorporating certain nonlocal effects²⁸ or accounting for the excitation process²⁹ have resulted in increase of as much as 0.5 eV, but much smaller effects are expected for metals. Some promising results have been obtained in a recent first-principles calculation of quasi-particle energies in silicon and diamond.³⁰ The calculation took account of nonlocal effects in the energy-dependent electron self-energy and also included local-field effects and dynamical screening. The results were in excellent agreement with experiment for the primary gap and most optical transitions. It is not obvious if such a calculation could account for the 0.4 eV discrepancy in Mg, but clearly a theoretical treatment more sophisticated than that of the electron gas is necessary.

The final states

Having determined the main features of the occupied bands, the next step in the analysis is, therefore, to investigate the final states. We will show below that these states are described rather well by single-particle calculations. Quantitatively, we observe differences between the positions of calculated and measured *d*-derived empty states as well as free-electron-like symmetry points. These discrepancies are such that they cannot be rectified by a simple linear scaling of the empty bands.

Before proceeding we must assign a k_{\perp} for each transition observed at an initial-state binding energy E_i . We do this by first assuming that the shape of the initial band is unchanged from that of the calculation of Chou and

Cohen.⁴ We then scale their results so that they agree with the measured symmetry point energies. This scaling follows the expression

$$E_i(k) = E_{\text{calc}}(k) - 0.65 - 0.14[E_{\text{calc}}(k) - E_{\text{calc}}(0)]. \quad (2)$$

Here, the first term [$E_{\text{calc}}(k)$] is the calculated binding energy at a wave vector k . The second term rigidly shifts

the calculated curve so as to yield the measured band bottom, while the third term makes a small linear correction to yield the experimental energy for the Γ_3^+ level. Since the high-lying initial-state band will not be used in the analysis of the final state below, it has not been rescaled.

By assuming vertical transitions, the final bands may be mapped from energy conservation: $E_f(k) = E_i(k) + \hbar\omega$.

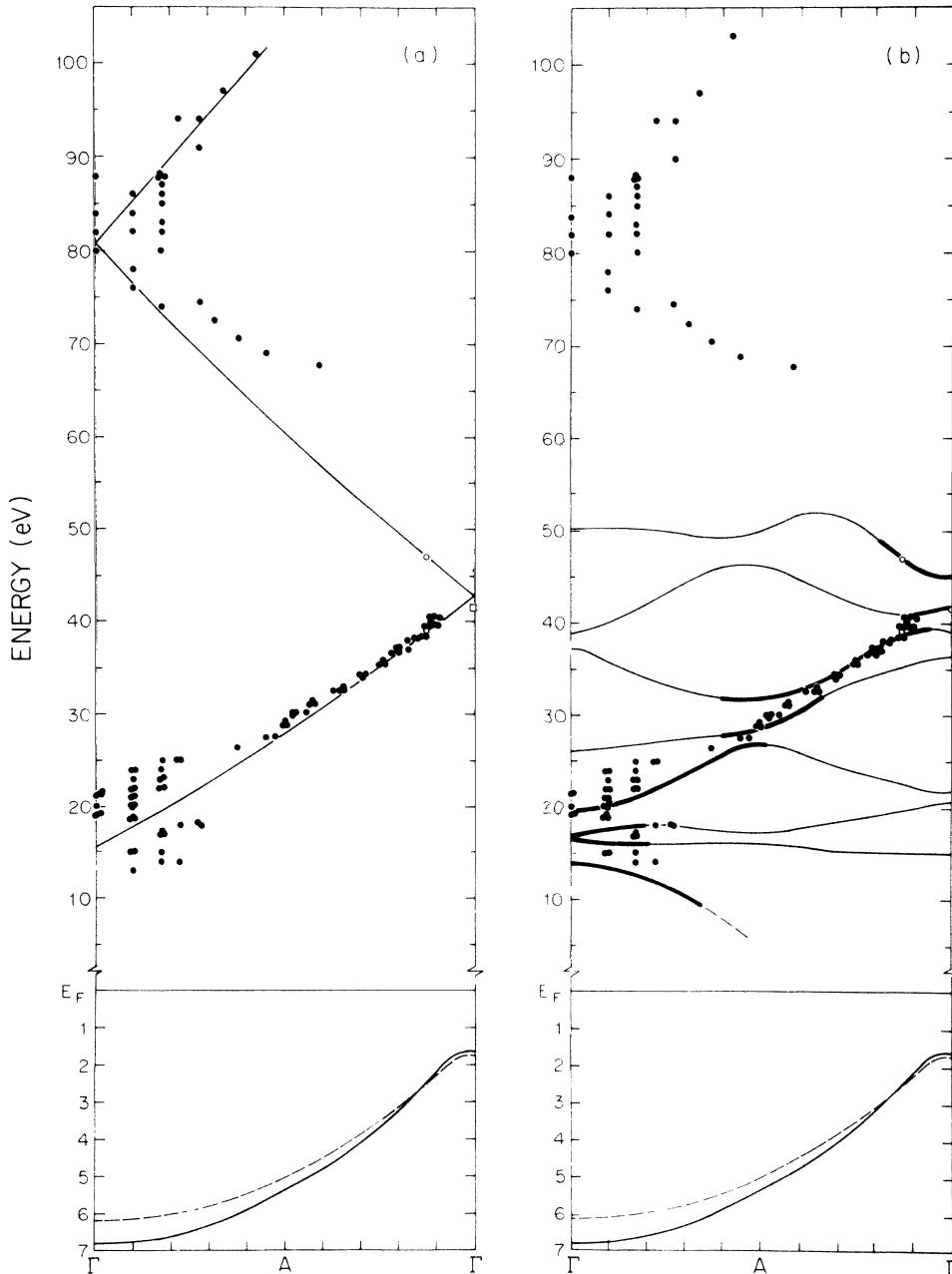


FIG. 10. The final bands of Mg along Δ . The points are derived from the scaled initial bands (see the text). The open circles are determined from the Fermi-level crossings (Fig. 5). The open square is the location of the resonance in the surface state (Fig. 3). The solid line below E_F shows the calculated bands of Chou and Cohen (Ref. 4), while the dashed line represents the same bands scaled to the measured symmetry points (see the text). The solid curve above E_F is a free-electron-like best fit to the final states with an effective mass $m^*/m = 1.04$ and originating 6.15 eV below E_F . In the right-hand panel, the calculated final states of Chou and Cohen (Ref. 4) are shown rigidly shifted upward by 4 eV. The heavy lines are bands expected to couple strongly to normal emission.

The final-state band structure derived in this manner is shown in Fig. 10. In each panel the solid line below E_F shows the original calculated band.⁴ The dashed line represents the rescaled bands used to generate the final states. We have incorporated all the bulk data including the two points in the final bands which are known from the Fermi-level crossings as well as the energy of the Γ_4^- point in the final state (given by the resonance in the surface-state cross section). There is very little scatter in the data for final energies above 28 eV and all the experimental points fall on a single smooth curve. The final bands in this region are best fit by a free-electron band with an effective mass $m^*/m=1.04$ originating 6.15 eV below E_F . This is shown in the left-hand panel of Fig. 10.

Below 28 eV, however, an erratic behavior is observed. This energy region corresponds to the photon energy range $19 \text{ eV} < \hbar\omega < 30 \text{ eV}$ in Fig. 6, where the bulk peak showed essentially no dispersion. In order to clarify whether these deviations are due to structure in the final or initial states, we have tested our data reduction procedure for self-consistency. We assign E versus k from the fitted free-electron band in Fig. 10 (left-hand panel), subtract $\hbar\omega$, and arrive at a new initial-state band that ideally should agree with the original assumption [Eq. (1)]. These results are shown in Fig. 11. The open circles are the results for the high-energy states, while the solid circles come from extrapolating the free-electron fit to energies below 28 eV. We see that the open circles agree rather well with the original assumption, given by the solid line, but the solid circles consistently lie below this curve. This leads us to believe that the erratic behavior has its origin in the final states.

The final states are understood more easily when compared to the calculation of Chou and Cohen.⁴ An excellent account of the high-energy free-electron-like states is given when their bands are rigidly shifted upward by 4 eV (right-hand panel of Fig. 10). In addition, the calculation shows flat, d -derived bands which occur some 18 eV

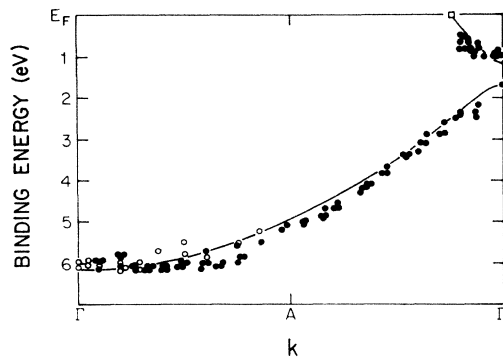


FIG. 11. The initial states along Δ as generated from the final states. The dots are generated from the final states below 28 eV, using an extrapolation of the free-electron band of Fig. 10. The open circles are generated from the final states above 28 eV. The solid curve shows the initial states of Chou and Cohen (Ref. 4) scaled to the measured symmetry points.

above E_F . This corresponds to the region of greatest deviation from the free-electron band in the left-hand panel of Fig. 10. Optical absorption data from the $2p$ core level¹³ show a large maximum approximately 20 eV above the Fermi level, attributable to transitions to unoccupied d states. It should be pointed out, however, that the predicted⁴ location of these states is still 3 eV too low, even with the 4-eV shift included in Fig. 10. This implies that a total upward shift of 7 eV would be required to bring these states into agreement with experiment. This shift is not due to energy-dependent self-energy effects. Such effects are expected to increase with greater electron energy,¹⁵ contrary to what has been observed here. The discrepancy could result from inadequate treatment of the d part of the potential used in the calculation.⁴ The d states could, in principle, be shifted in the $2p$ adsorption spectrum due to the attractive potential from the core hole. We reject this possibility, however, as there is good agreement between the positions of the optical-absorption peak and of the empty d states seen in photoemission.

Surface states

Resonances in the photoexcitation cross sections of surface states can originate from different effects. At low photon energies, near the plasmon energy, resonances have been observed for surface emission from Al(100),³¹ Be(0001),³ and for thin alkali-metal films.³² These have been attributed to variations in the electromagnetic field at the surface as the photon energy passes through the threshold for plasmon production.^{3,31,32} As the plasmon energy of Mg is 10.5 eV, this effect can have no influence on the data in Fig. 3.

Alternatively, a resonance can result from strong coupling of the surface-state wave function to that of a particular final state. This phenomenon was first recognized by Louie *et al.*³³ If a surface state at a particular k_{\parallel} is split off by a small amount from the bulk band edge at that k_{\parallel} , its wave function will be very similar to that of the band edge. When strong bulk transitions are allowed from this edge to a particular final state, the surface-state intensity will also be enhanced. In addition to Cu(111) (Ref. 33), such enhancements have been observed on Al(100) (Ref. 2) and Al(111) (Ref. 34). On Be(0001) (Ref. 3), where the surface state is split off far from the bulk bands, no single bulk state dominates the wave function and no large enhancements are observed.

The high-energy resonance in Fig. 3 is a direct reflection of the surface-state wave function and corresponds closely to previously observed surface-state resonances.^{3,33,34} The $\bar{\Gamma}$ surface state is split off from the Γ_3^+ bulk state by only 0.1 eV. This implies that its wave function has a large component of Γ_3^+ symmetry.³⁵ When the photon energy is high enough to reach the Γ_4^- level in the final state, the surface state resonates due to the favorable $\Gamma_3^+ \rightarrow \Gamma_4^-$ dipole coupling. This allows us to locate the energy of Γ_4^- from the maximum of the resonance at $43 \text{ eV} - 1.6 \text{ eV} = 41.4 \text{ eV}$ above E_F .

By assuming a free-electron-like dispersion for the final states, the energy scale of Fig. 3 can be represented in terms of the perpendicular momentum (k_{\perp}) (top of Fig.

3). The resonance is very narrow on this scale, which implies that only states within about 0.1 of the BZ about Γ_3^+ have an appreciable contribution to the surface-state wave function.

The low-energy resonance seen in Fig. 3 occurs at energies corresponding to the unoccupied d bands discussed above. As the surface state is very close to the p -like Γ_3^+ state, its wave function will, in a localized picture, have strong p character. The strong $p \rightarrow d$ coupling consequently leads to the enhancement.

The surface-state behavior away from normal emission shows several interesting features. In Fig. 4 it is evident that the intensity of the surface state at \bar{M} is considerably greater than at $\bar{\Gamma}$. This can be understood in the same way as the high-energy resonance at $\bar{\Gamma}$. In the spectra near $\theta = 30^\circ$ in Fig. 4 a bulk feature is seen dispersing to a binding energy of about 1.5 eV, very close to the projected band edge. As the \bar{M} surface state is also near the band edge, it couples strongly to the same final states as the bulk band edge and is enhanced. It is interesting to note that at higher photon energies, the \bar{M} surface-state intensity is much smaller so as to be almost indistinguishable from the background near $\hbar\omega = 40$ eV.

When the dispersions of the surface states are compared to the projected bulk bands in Fig. 5, the surface state is seen to lie on the calculated bulk band edge⁴ for almost its entire range. As we saw above, however, data from bulk emission show that the energy of the Γ_3^+ state is 1.7 eV, which would place the bottom of the gap 0.1 eV deeper. Since the surface-state line shape does not change significantly throughout its dispersion, it is unlikely that it crosses the band edge. For Be(0001),³ it was observed that the line shape changed drastically when the surface state became a surface resonance upon overlapping the projected bulk bands.

There is an important qualitative difference between the surface states on Mg(0001) and Be(0001) near \bar{M} . On Be (Ref. 3), two surface states are observed at \bar{M} while only one is seen on Mg. As discussed elsewhere,^{3,36} a gap of the type existing at \bar{M} may support either one or two surface states. The exact number depends on the value of several material-dependent parameters. The \bar{M} gap of Mg is approximately an order of magnitude smaller than on Be, which greatly reduces the likelihood of a second surface state in that gap.

Peak widths

Peak widths in photoemission are of interest because they are related to the electron and hole lifetimes. This relationship may be expressed by the approximate formula²¹

$$W = [(2\Gamma_{\text{hole}})^2 + (2R\Gamma_{\text{el}})^2]^{1/2}. \quad (3)$$

Here, W is the peak width, $\hbar/2\Gamma_{\text{hole}}$ and $\hbar/2\Gamma_{\text{el}}$ are the hole and electron lifetimes, respectively, and R is the ratio of the slopes ($\partial E/\partial k$) of the initial- and final-state bands. If a regime of parameters exists, where one of the contributions to the width is small, Eq. (3) may be applied to

determine the other lifetime directly. For example, if the factor R is very small (i.e., a transition from a flat initial band to a steep final band), then the second term in Eq. (3) may be neglected and the peak width is essentially a measure of the hole lifetime. This was the case for Be where the peak widths decreased continuously as $k/k_F \rightarrow 1$ and, over at least part of the investigated range, agreed well with electron-gas calculations.³ The situation in Mg is more complicated. It is evident from Fig. 9 that the peak widths are much larger than can be accounted for by the hole lifetimes. Macroscopic roughness of the sample surfaces could lead to a broadening of the peak widths via diffuse scattering at the surface. However, the sharpness of the surface state, its symmetric behavior, and the quality of the LEED pattern indicate that the surface is microscopically well ordered and the observed peak widths are an intrinsic property of Mg.

In the energy range investigated, the experimentally measured dispersions show that $\frac{1}{10} < R < \frac{1}{3}$. The electron lifetime grows rapidly enough to keep the peak widths nearly constant throughout the entire range measured as shown in the data for the (11 $\bar{2}$ 0) surface in the top panel of Fig. 9. For $k/k_F > 0.5$, the predicted hole lifetime falls off quickly, which accounts for the slight reduction in width observed.

The simplicity of the initial states and the regular behavior of the peak widths in the [11 $\bar{2}$ 0] direction lead us to suspect that the final-state band structure along [0001] may be responsible for the variation in the peak widths from the [0001] direction (Fig. 9). From the right-hand panel of Fig. 10 we see that for transitions near $k_\perp = 0.5$ ($\hbar\omega \approx 35$ eV), the final states exhibit several gaps between bands which are considerably flatter than the neighboring free-electron-like bands. Assuming initial-state lifetimes as predicted by electron-gas theory (Fig. 9, solid curve), reasonable final-state lifetimes for these energies (see below), and the band dispersions of Fig. 10, the peak widths along Δ can be calculated from Eq. (3). The result is given by the dashed curve in the lower panel of Fig. 9. This simple approach reproduces the general trends of the data. A more sophisticated analysis, including the imaginary part of the band structure, would be necessary to understand the width variation in detail, but the major contribution seems to have been identified.

A measure of the final-state (electron) lifetime may be obtained in a region where the hole lifetime is very long. This situation occurs near E_F as is indicated by the solid lines in Fig. 9. As the Fermi level is approached, the phase space for low-energy excitations becomes vanishingly small and the hole lifetime goes to infinity. By observing transitions which occur at the Fermi level, the final-state lifetime may be measured as a transition crosses E_F . A plot of the Fermi-level intensity as a function of photon energy is presented in Fig. 8. After subtraction of a linear background, the two-peaked structure can be fit very well by two Lorentzian peaks, one at $\hbar\omega = 39$ eV (FWHM 4.2 ± 0.4 eV) and one at $\hbar\omega = 47$ eV (FWHM 5.0 ± 0.5 eV). As we are examining the emission intensity $I(E_i, \hbar\omega)$ at a constant initial energy E_i as the photon energy $\hbar\omega$ is varied, Eq. (3) is no longer applicable. Instead, we use the relation presented by Eastman and co-workers³⁷

$$I(E_i, \hbar\omega) \propto \frac{\Gamma_{el}(E_f)/2}{(\hbar\omega - \hbar\omega_0)^2 + [\Gamma_{el}(E_f)/2]^2}, \quad (4)$$

where $\hbar\omega = E_f - E_i$. This shows that the final-state lifetime is given directly by the widths of the Lorentzians in Fig. 8. Our values are slightly smaller than those determined for Al (Ref. 2) (4.5 eV at 40 eV above E_F) and Zn (Ref. 38) (5.5 eV at about 48 eV above E_F), but not significantly so.

CONCLUSIONS

We have measured the bulk and surface electronic behavior of Mg(0001) and (11 $\bar{2}$ 0). The occupied band energies at Γ are given by $\Gamma_1^+ = 6.15 \pm 0.1$ eV, $\Gamma_3^+ = 1.7 \pm 0.1$ eV, and $\Gamma_4^- = 0.9 \pm 0.1$ eV. When compared to local-density pseudopotential calculations,⁴ the bandwidth is about 10% narrower than calculated, while the $\Gamma_3^+ - \Gamma_4^-$ gap is about twice as wide as predicted. Final-state band dispersions show free-electron-like behavior for final energies greater than 28 eV above the Fermi level. For lower final-state energies, large deviations from free-electron-like behavior are attributed to transitions to unoccupied d states. Measured peak widths indicate that the hole lifetimes are greater than those predicted by an interacting electron gas calculation.¹⁵ The electron lifetimes are in accord with results from other materials. In general, we

find the basic features of the photoelectron spectra are accounted for by a direct transition model employing a density functional band-structure calculation.⁴ Detailed agreement does not exist, however, and may in part be traced to the fact that photoemission involves excitations of the system.

Surface states have been observed near the $\bar{\Gamma}$ and \bar{M} symmetry points of the surface Brillouin zone. The state at $\bar{\Gamma}$ has a binding energy of 1.6 ± 0.1 eV, which is approximately 0.1 eV shallower than previously reported.¹⁶ The photoexcitation cross section of this state shows a sharp resonance corresponding to transitions to a final state of Γ_4^- symmetry. The \bar{M} surface state shows a similar resonance at $\hbar\omega = 26$ eV and has a binding energy of 1.1 ± 0.1 eV.

ACKNOWLEDGMENTS

We thank Dr. M. Y. Chou and Dr. M. L. Cohen for generously sharing with us the results of their extensive calculations of the band structure of Mg, and Dr. E. Jensen for many helpful discussions. This research was supported by the National Science Foundation Materials Research Laboratory Program under Grant No. DMR-82-16718. The storage ring Tantalus II is supported by the National Science Foundation under Grant No. DMR-80-20164.

- ¹E. W. Plummer and W. Eberhardt, *Adv. Chem. Phys.* **49**, 533 (1982); F. J. Himpsel, *Adv. Phys.* **39**, 1 (1983), and references therein.
- ²H. J. Levinson, F. Greuter, and E. W. Plummer, *Phys. Rev. B* **27**, 727 (1983).
- ³E. Jensen, R. A. Bartynski, T. Gustafsson, and E. W. Plummer, *Phys. Rev. Lett.* **52**, 2172 (1984); E. Jensen, R. A. Bartynski, T. Gustafsson, E. W. Plummer, M. Y. Chou, M. L. Cohen, and G. B. Hoflund, *Phys. Rev. B* **30**, 5500 (1984); R. A. Bartynski, E. Jensen, T. Gustafsson, and E. W. Plummer, *Phys. Rev. B* **32**, 1921 (1985).
- ⁴M. Y. Chou and M. L. Cohen (private communication).
- ⁵L. M. Falicov, *Philos. Trans. R. Soc. London, Ser. A* **255**, 55 (1962).
- ⁶J. C. Kimball, R. W. Stark, and F. M. Mueller, *Phys. Rev.* **162**, 600 (1967).
- ⁷J. O. Dimmock, in *Solid State Physics*, edited by F. Seitz, P. Turnbull, and H. Ehrenreich (Holt, Reinhardt and Winston, New York, 1971), Vol. 26, p. 212–219.
- ⁸S. Chatterjee and P. Shina, *J. Phys. F* **5**, 2089 (1975).
- ⁹R. Asokamani, K. Iyakutti, R. S. Rao, and V. Devanathan, *J. Phys. F* **8**, 2323 (1978).
- ¹⁰S. Wakoh, *J. Phys. Soc. Jpn.* **50**, 490 (1981).
- ¹¹R. D. Gupta and A. J. Freeman, *Phys. Rev. Lett.* **36**, 1194 (1976).
- ¹²L. Wilk, W. R. Fehler, and S. H. Vosko, *Can. J. Phys.* **56**, 266 (1978).
- ¹³H.-J. Hagemann, W. Gudat, and C. Kunz, *J. Opt. Soc. Am.* **65**, 742 (1975).
- ¹⁴U. O. Karlsson, G. Hansson, P. Persson, and S. A. Flodström, *Phys. Rev. B* **26**, 1852 (1982).
- ¹⁵L. Hedin and S. Lundqvist, in *Solid State Physics*, edited by F. Seitz, P. Turnbull, and E. Ehrenreich (Holt, Reinhardt and Winston, New York, 1969), Vol. 23, p. 1.
- ¹⁶B. P. Tonner, *Nucl. Instrum. Methods* **172**, 133 (1980).
- ¹⁷C. L. Allyn, T. Gustafsson, and E. W. Plummer, *Rev. Sci. Instrum.* **49**, 1197 (1978).
- ¹⁸C. Herring, *J. Franklin Inst.* **233**, 525 (1942).
- ¹⁹J. B. Ketterson and R. W. Stark, *Phys. Rev.* **156**, 748 (1967).
- ²⁰R. W. Stark, *Phys. Rev.* **162**, 589 (1967).
- ²¹J. B. Pendry, in *Photoemission and the Electronic Properties of Surfaces*, edited by B. Feuerbacher, B. Fitton, and R. F. Willis (Wiley, New York, 1978), p. 64.
- ²²E. Jensen and E. W. Plummer, *Phys. Rev. Lett.* **55**, 1912 (1985).
- ²³P. Thiry, D. Chandesris, J. Lecante, C. Guillot, R. Pinchaux, and Y. Petroff, *Phys. Rev. Lett.* **43**, 82 (1979).
- ²⁴J. F. Janak, A. R. Williams, and V. L. Moruzzi, *Phys. Rev. B* **11**, 1522 (1975).
- ²⁵J. P. Perdew and A. Zunger, *Phys. Rev. B* **23**, 5048 (1981).
- ²⁶M. R. Norman, *Phys. Rev. B* **29**, 2956 (1984).
- ²⁷F. Sacchetti, *J. Phys. F* **12**, 281 (1982).
- ²⁸G. P. Kerker, *Phys. Rev. B* **24**, 3468 (1981).
- ²⁹C. S. Wang and W. E. Pickett, *Phys. Rev. Lett.* **51**, 597 (1983).
- ³⁰M. S. Hybertsen and S. G. Louie, *Phys. Rev. Lett.* **55**, 1418 (1985).
- ³¹H. J. Levinson, E. W. Plummer, and P. J. Feibelman, *Phys. Rev. Lett.* **43**, 952 (1979).
- ³²Lars Walldén, *Phys. Rev. Lett.* **54**, 943 (1985).
- ³³S. G. Louie, P. Thiry, R. Pinchaux, Y. Petroff, D. Chandesris, and J. Lecante, *Phys. Rev. Lett.* **44**, 549 (1980).
- ³⁴S. D. Kevan, N. G. Stoffel, and N. V. Smith, *Phys. Rev. B* **31**,

- 1788 (1985).
- ³⁵E. T. Goodwin, Proc. Cambridge Philos. Soc. **35**, 221 (1939).
- ³⁶R. A. Bartynski, T. Gustafsson, and Paul Soven, Phys. Rev. B **31**, 4745 (1985).
- ³⁷D. E. Eastman, J. A. Knapp, and F. J. Himpsel, Phys. Rev. Lett. **41**, 825 (1978).
- ³⁸F. J. Himpsel, D. E. Eastman, and E. E. Koch, Phys. Rev. B **24**, 1687 (1981).